Synchronization of chaotic resonators based on control theory

T. C. Newell,* P. M. Alsing,† A. Gavrielides,‡ and V. Kovanis§
Nonlinear Optics Center, Phillips Laboratory, PL/LIDN, 3550 Aberdeen Avenue SE, Kirtland Air Force Base, New Mexico 87117-5776
(Received 21 November 1994)

We have investigated experimentally and computationally a synchronization scheme, based on control theory, for the case of two nearly identical chaotic diode resonators. From the experimentally captured time series we calculate the required feedback factors and explain why this factor can also be approximated as a constant for the duration of its application. Both the calculated and constant feedback factors are implemented experimentally in order to synchronize two resonators. In addition, we observe that the application of the perturbing factor was only necessary when the resonator was in the unstable region of the attractor.

PACS number(s): 05.45.+b, 84.30.Wp

I. INTRODUCTION

The publication of two seminal papers in 1990 altered the focus of research in chaotic dynamical systems. Instead of studying the possible implications of the sensitive dependence to initial conditions, theoretical and experimental studies are now exploiting that very property in order to *control* [1] or *synchronize* [2] the output of chaotic systems. The growing interest in synchronizing chaotic signals is driven by the potentiality for applications to secure communications [3], designing arrays of coupled chaotic lasers [4], developing cardiac pacemakers, and other biomedical applications [5]. Currently two major approaches to chaotic synchronization have been studied in the literature. The method of Pecora and Carroll [2] involves isolating from a chaotic system a subsystem which contains only negative Lyapunov exponents. A pair of identical subsystems can then be synchronized by a chaotic driving component of the full system. Another approach, loosely referred to as synchronization by *continuous feedback* [6], involves the continuous feedback of a component signal difference multiplied by a proportionality factor to either a slave system (unidirectional synchronization) or to both a master and slave system (mutual synchronization). In this method the value of the proportionality factor is not known from experimental data *a priori* and must be determined empirically.

In this paper we explore a third approach to chaotic synchronization developed by Lai and Grebogi [8]. This method is a direct extension of the techniques used successfully by Ott, Grebogi, and Yorke (OGY) [1] to control unstable periodic orbits. For a comprehensive review of various aspects and applications of the OGY method, the reader should consult Refs. [7]. The synchronization procedure of Lai and Grebogi requires making minute controlling perturbations to a control parameter of a slave chaotic system in order to steer its orbit onto a master chaotic orbit. Motivated by their work, the authors recently demonstrated synchronization using a proportional feedback scheme applied to a pair of chaotic diode resonator circuits [9]. Synchronization was achieved by modulating the amplitude of the drive wave of one of the resonators with a controlling feedback signal. This signal was proportional to the voltage difference between the two resonators and was applied for a fraction of the driving cycle. Their method is the synchronization analog of the occasional proportional feedback scheme developed by Hunt [12] for controlling unstable periodic orbits.

The focus of this paper is to apply the control theory method of synchronization to the case of nearly identical chaotic diode resonators. We numerically demonstrate, through the calculation of Lyapunov multipliers, that while the theoretically prescribed feedback minimizes the conditional global Lyapunov multiplier, simplifications of the formula will also induce synchronization. Experimentally, we implement the control theory synchronization procedure in a pair of diode resonators circuits. We also show experimentally that synchronization can be achieved when the control feedback is applied only when the resonator trajectory is traversing an unstable region of the attractor.

This paper is organized as follows. The Lai and Grebogi synchronization scheme is reviewed in Sec. II. In Sec. III we introduce the dynamical system describing the chaotic diode resonator. In Sec. IV we numerically investigate how the conditional local Lyapunov multipliers change when two diode resonators are synchronized using control theory. In Sec. V we demonstrate how the required synchronizing factors can be extracted from the experimentally obtained return map. Two experiments are described in Sec. VI. The first is an implementation of the Lai and Grebogi scheme using the prescribed feedback to obtain synchronization. The second shows that synchronization can be achieved when feedback is applied only if the system is in an unstable region of the attrac-

*Electronic address: newell@hpruby.plk.af.mil
†Electronic address: alsing@arom.plk.af.mil
‡Electronic address: tom@photon.plk.af.mil
§Electronic address: kovanis@xaos.plk.af.mil

tor. The main points are summarized and conclusions are drawn in Sec. VII. Finally the dynamical equations describing the diode resonator circuit are derived in the Appendix.

II. SYNCHRONIZATION USING CONTROL

The OGY method for controlling unstable periodic orbits requires perturbing a control parameter of a chaotic system in order to stabilize one of the unstable periodic orbits. Perturbations are periodically computed based on the difference between the point of crossing of the chaotic orbit through a Poincaré section and a fixed point in this section. The Lai and Grebogi technique of synchronization using control also calls for periodically making a minute perturbation to an existing control parameter of a chaotic system. However in this case, the required perturbation is based on the difference between a slave orbit and a freely operating chaotic master system when they cross a Poincaré section. Figure 1 graphically depicts the effect of the perturbation on the slave orbit.

The synchronization formula is derived by considering two k-dimensional mappings $\boldsymbol{x}_{n+1} = \boldsymbol{F}(\boldsymbol{x}_n, p_0)$ and $\boldsymbol{y}_{n+1} = \boldsymbol{F}(\boldsymbol{y}_n, p)$, where the former (master) depends on a fixed parameter p_0 while the latter (slave) depends on a control parameter p to which synchronizing perturbations are applied. To generate the stabilizing feedback, we first identify the stable and unstable manifolds [for our case consider only one stable and one unstable direction, $\boldsymbol{f}_{s(n)}$ and $\boldsymbol{f}_{u(n)}$] of the chaotic dynamical system. In general, these eigenvectors will rotate in some manner governed by the underlying dynamics of the system as the orbit wanders along the attractor. This requires some knowledge of the mapping so that a small sphere of points can be propagated forward in time in order to estimate this unstable direction [8,10]. If we expand the slave orbit locally about the master and apply the requirement that $[\boldsymbol{y}_{n+1} - \boldsymbol{x}_{n+1}] \cdot \boldsymbol{f}_{u(n+1)} = 0$, then the perturbation necessary to synchronize $\boldsymbol{y}_n$ to $\boldsymbol{x}_n$ is given by [8]

$$\delta p_n = \left. \frac{[\boldsymbol{D}_{\boldsymbol{y}}\boldsymbol{F}(\boldsymbol{y},p) \cdot \{\boldsymbol{y}_n - \boldsymbol{x}_n(p_0)\} \cdot \boldsymbol{f}_{u(n+1)}]}{-\boldsymbol{D}_p\boldsymbol{F}(\boldsymbol{y},p) \cdot \boldsymbol{f}_{u(n+1)}} \right|_{\boldsymbol{y}=\boldsymbol{x},p=p_0}, \tag{2.1}$$

where the derivative terms are evaluated at $\boldsymbol{y}_n = \boldsymbol{x}_n, p = p_0$. In principle the perturbation is to be applied whenever it is a small fraction of the unperturbed parameter. Hence, one should not apply the feedback if the separation between the two orbits is large or the denominator of Eq. (2.1) is small. The parameter p is changed to $p_n = p_0 + \delta p_n$ upon the nth crossing of the surface of section. For a continuous flow the parameter should be held constant at p_n until the next, $(n+1)$th crossing of the surface of section, at which time it is changed again.

The physical interpretation of this formula is straightforward. The proximity of the slave orbit to the master is amplified by a factor which is directly proportional to the rate of growth or contraction of the master-slave separation in the unstable direction, and inversely proportional to the sensitivity of the map to a variation in the control parameter. Naturally, the greater the rate of divergence of the orbits the larger the perturbation factor must be. Also, a map with a sensitive dependence to the control parameter requires a relatively small perturbation.

The above method of Lai and Grebogi achieves synchronization by setting the local rate of divergence of the master-slave orbit in the unstable direction to zero at each iteration of the map. Note that for systems with more than one positive Lyapunov exponent, this criterion alone does not, in general, guarantee synchronization. As pointed out by So and Ott [11], for high dimensional systems the product of the eigenvalues of the Jacobian matrices is not necessarily equal to the eigenvalue of the product of the Jacobian matrices. In such systems the scalar feedback defined in Eq. (2.1) is not likely to be successful.

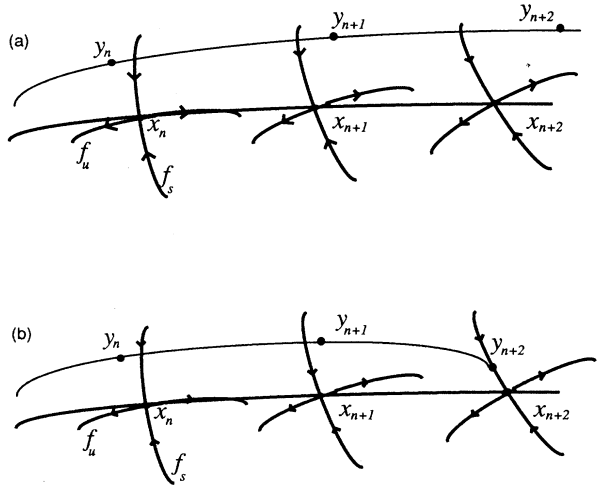

FIG. 1. (a) While the unperturbed slave orbit, $\boldsymbol{y}$, may approach the master orbit, $\boldsymbol{x}$, eventually it will move off along the unstable direction, $\boldsymbol{f}_{u(n)}$. (b) By applying the appropriate perturbations to the $\boldsymbol{y}$ slave system, we direct its orbit so that it has no component along the unstable direction, $\boldsymbol{f}_u$, of the $\boldsymbol{x}$ master orbit. The $\boldsymbol{y}$ orbit then approaches the $\boldsymbol{x}$ orbit along the stable direction $\boldsymbol{f}_s$.

III. THE DRIVEN CHAOTIC *RLC* CIRCUIT

The system under study is a driven nonlinear *RLC* circuit composed of a 1N4004 silicon rectifier diode, a 33 mH inductor (dc resistance 243 Ω), and a 90.5 Ω resistor in series. It is sinusoidally driven at a frequency of 70 kHz. The nonlinearity of the system arises from the nonlinear conduction and capacitance properties of the diode.

In the past the diode resonator was used as a paradigm to observe various chaotic phenomena. It has displayed the *period doubling* route into chaos [13], *tangent* bifurcations [14], an *intermittent* route to chaos [15], and *crisis* [16,17]. Other studies of the circuit revealed forward and reverse bifurcations with respect to the drive *voltage*

[18,19], drive *frequency* [20], *wave bias* [21], and diode temperature [22].

The equations of motion for the circuit are derived from Kirchoff's laws [23,24]. In terms of the dimensionless current, $\mathcal{I}$, and voltage drop across the diode, $\mathcal{V}$, these are

$$\frac{d\mathcal{I}}{d\tau} = \mathcal{V}_0 \sin(\tau) + \mathcal{V} - \frac{\mathcal{I}}{\beta},$$
$$\frac{d\mathcal{V}}{d\tau} = G(\mathcal{I},\mathcal{V}) \tag{3.1}$$

where

$$G(\mathcal{I},\mathcal{V}) = \begin{cases} \frac{\mathcal{I}-\gamma(e^{\alpha\mathcal{V}}-1)}{c_1[e^{\alpha\mathcal{V}}+c_2(1-\mathcal{V})^{-m}]} & \text{if } \mathcal{V} < \frac{1}{2}, \\ \frac{\mathcal{I}-\gamma(e^{\alpha\mathcal{V}}-1)}{c_1[e^{\alpha\mathcal{V}}+c_2\frac{(b_2+m\mathcal{V})}{b_1}]} & \text{if } \mathcal{V} \geq \frac{1}{2}. \end{cases} \tag{3.2}$$

For our particular system, the constants are $\beta = 43.5$, $\alpha = 7.69$, $\gamma = 0.257$, $b_1 = 0.384$, $b_2 = 0.31$, $c_1 = 4.26$, $c_2 = 0.078$, and $m = 0.38$. A derivation of these equations is given in the Appendix.

Figures 2(a) and 2(b) are plots of bifurcation diagrams of the current versus the drive wave amplitude. Both Figs. 2(a) (numerically calculated) and 2(b) (experimentally measured) clearly show period doubling cascades into chaos. The model is in excellent qualitative agreement with that measured experimentally and in good quantitative agreement [25]. In this work, we report results obtained from the chaotic region below the period-3 window.

The two nonzero Lyapunov exponents, obtained from the model, are shown in Fig. 3(a) for a range of drive voltages. They show the ascent into chaos along with various windows of stability. A zero value delineates the chaotic regime from the periodic and quasiperiodic regions. Figure 3(b) displays the Kaplan-Yorke conjecture [26] for the fractal dimension of the attractor.

In order to apply the synchronization scheme of Lai and Grebogi we need to determine the unstable contravariant eigenvector, $\boldsymbol{f}_{u(n)}$, at each crossing of the orbit trajectory through a Poincaré section of the attractor. We define this Poincaré section as the peaks of the resonator current ($\dot{\mathcal{I}} = 0$, $\ddot{\mathcal{I}} < 0$). Since the dynamical variables of our diode resonator are the circuit current $\mathcal{I}$ and the diode voltage drop $\mathcal{V}$, $\boldsymbol{f}_u$ will have components $\boldsymbol{f}_{u(n)} = (f_{\mathcal{I}(n)}, f_{\mathcal{V}(n)})$ at the nth crossing. Defining the difference between the slave signal $\boldsymbol{y}_n$ and the master signal $\boldsymbol{x}_n$ as $\boldsymbol{\epsilon}_n \equiv \boldsymbol{y}_n - \boldsymbol{x}_n$, Eq. (2.1) can be written as

$$\delta p_n \equiv \boldsymbol{\alpha}_n \cdot \boldsymbol{\epsilon}_n \tag{3.3}$$
$$= -\frac{f_{u\mathcal{I}(n+1)}\,J_{11(n)} + f_{u\mathcal{V}(n+1)}\,J_{21(n)}}{f_{u\mathcal{I}(n+1)}\,V_{\mathcal{I}(n)} + f_{u\mathcal{V}(n+1)}\,V_{\mathcal{V}(n)}}\,\epsilon_{\mathcal{I}(n)}$$
$$-\frac{f_{u\mathcal{I}(n+1)}\,J_{12(n)} + f_{u\mathcal{V}(n+1)}\,J_{22(n)}}{f_{u\mathcal{I}(n+1)}\,V_{\mathcal{I}(n)} + f_{u\mathcal{V}(n+1)}\,V_{\mathcal{V}(n)}}\,\epsilon_{\mathcal{V}(n)}. \tag{3.4}$$

In the above formula we have written the components of the 2×2 Jacobian matrix $\boldsymbol{D_y F}$ as $J_{ij(n)}$ and the components of the shift vector $\boldsymbol{D_p F}$ as $(V_{\mathcal{I}(n)}, V_{\mathcal{V}(n)})$ at the nth iteration. In general $\boldsymbol{\alpha}$ is a vector quantity. However, for our choice of the Poincaré section, the diode voltage drop

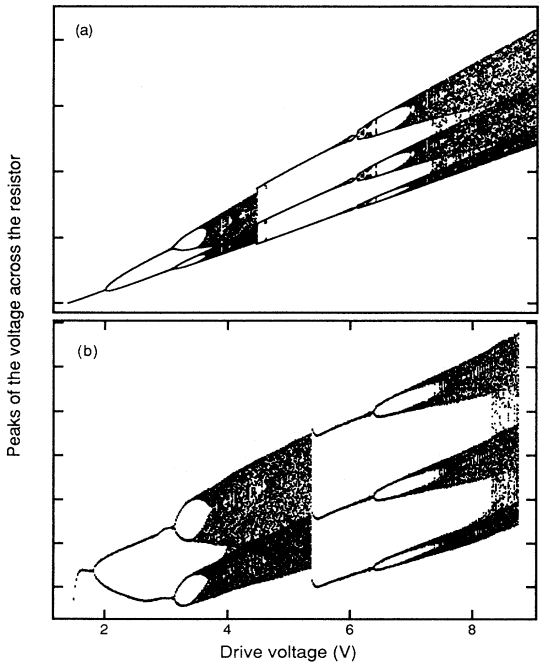

FIG. 2. Bifurcation diagrams of the current through the circuit as a function of the drive voltage calculated (a) numerically from Eq. (3.1) and Eq. (3.2) and (b) from experimental data. Observe that we obtain very good qualitative agreement between theory and experiment.

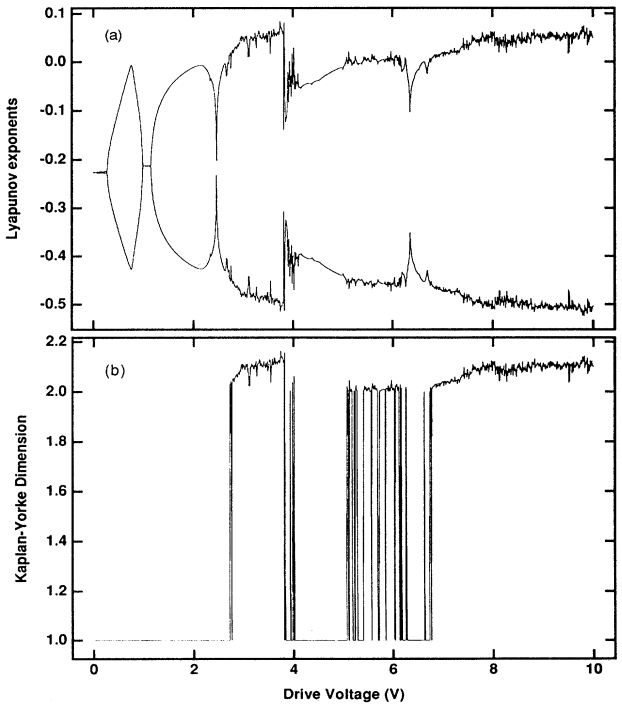

FIG. 3. (a) The Lyapunov exponents λ_1 and λ_3 ($\lambda_2 = 0$) are numerically calculated as a function of the wave amplitude, $\mathcal{V}_0$. (b) The Kaplan-Yorke conjecture for the attractor dimension.

staturates to a level of approximately 0.7 V. Thus upon each iteration, the error $\epsilon_{\mathcal{V}(n)}$ in the master-slave diode voltages is negligible, and the second line of Eq. (3.4) does not contribute to δp_n.

To determine the remaining contributions to δp_n in Eq. (3.4) we need to calculate the unstable direction $\boldsymbol{f}_{u(n)}$ and the components of the Jacobian $J_{11(n)} = \partial\mathcal{I}_{n+1}/\partial\mathcal{I}_n$ and $J_{21(n)} = \partial\mathcal{V}_{n+1}/\partial\mathcal{I}_n$. The latter can be performed numerically by perturbing the diode resonator values at a given peak n from $(\mathcal{I}_n, \mathcal{V}_n) \rightarrow (\mathcal{I}'_n = \mathcal{I}_n + \delta, \mathcal{V}'_n = \mathcal{V}_n)$ and at the next peak estimating the derivative to be approximately $J_{11(n)} \approx (\mathcal{I}'_{n+1} - \mathcal{I}_n)/\delta$. Similarly by perturbing the peaks via $(\mathcal{I}_n, \mathcal{V}_n) \rightarrow (\mathcal{I}'_n = \mathcal{I}_n, \mathcal{V}'_n = \mathcal{V}_n + \delta)$ we have $J_{21(n)} \approx (\mathcal{V}'_{n+1} - \mathcal{V}_n)/\delta$. The shifts $\boldsymbol{D}_p\boldsymbol{F} = (V_{\mathcal{I}(n)}, V_{\mathcal{V}(n)})$ can likewise be determined by starting with the initial conditions $(\mathcal{I}_n, \mathcal{V}_n)$ at the nth peak and perturbing the control parameter (V_0) from $p_0 \rightarrow p_0 + \delta$ and estimating the derivatives similarly.

To determine the unstable directions numerically we can proceed in a manner similar to that defined in [8,10]. By propagating a unit vector $\boldsymbol{e}$ from peak $n-1$ to peak n via the linearization of the diode resonator equations, we obtain an estimate of the direction $\boldsymbol{e}_u$ of the unstable manifold at the nth peak. Similarly, by propagating a unit vector backwards in time from peak $n+1$ to peak n via the time reversed version of the linearized diode resonator equations, we obtain an estimate for the direction $\boldsymbol{e}_s$ of the stable manifold at the nth peak. We can then solve for the contravariant versions of these vectors $\boldsymbol{f}_u$ and $\boldsymbol{f}_s$ from the conditions $\boldsymbol{f}_u \cdot \boldsymbol{e}_u = 1$, $\boldsymbol{f}_s \cdot \boldsymbol{e}_s = 1$ and $\boldsymbol{f}_u \cdot \boldsymbol{e}_s = 0$, $\boldsymbol{f}_s \cdot \boldsymbol{e}_u = 0$.

Upon performing this analysis we find

$$\left|\frac{f_{u\mathcal{V}(n+1)}\, J_{21(n)}}{f_{u\mathcal{I}(n+1)}\, J_{11(n)}}\right| \ll 1 \qquad \text{and} \qquad \left|\frac{f_{u\mathcal{V}(n+1)}\, V_{\mathcal{V}(n)}}{f_{u\mathcal{I}(n+1)}\, V_{\mathcal{I}(n)}}\right| \ll 1,$$

across the whole attractor, so that components along the diode voltage contribute much less significantly to δp_n than the components along the circuit current. This allows us to approximate the perturbation formula as

$$\delta p_n = -\frac{J_{11(n)}}{V_{\mathcal{I}(n)}}\,\epsilon_{\mathcal{I}(n)} = -\frac{\partial\mathcal{I}_{n+1}/\partial\mathcal{I}_n}{\partial\mathcal{I}_{n+1}/\partial p_n}\,\epsilon_{\mathcal{I}(n)}. \tag{3.5}$$

It is significant to note that all references to the contravariant vector $\boldsymbol{f}$ have canceled in the above perturbation formula. Equation (3.5) is the appropriate Lai-Grebogi formula for a one-dimensional map of the form $\mathcal{I}_{n+1} = \boldsymbol{F}(\mathcal{I}_n, p)$. This is consistent with our estimated value of 1.16 for the Kaplan-Yorke dimension of diode resonator attractor on the surface of section. The nearly one-dimensional nature of the attractor is evident from the thinness of the first return map as shown in Fig. 4. Experimentally, Eq. (3.5) translates into a much simpler formula to implement as opposed to the full vector form of the perturbation, Eq. (2.1) involving the direction of the unstable manifold at each peak.

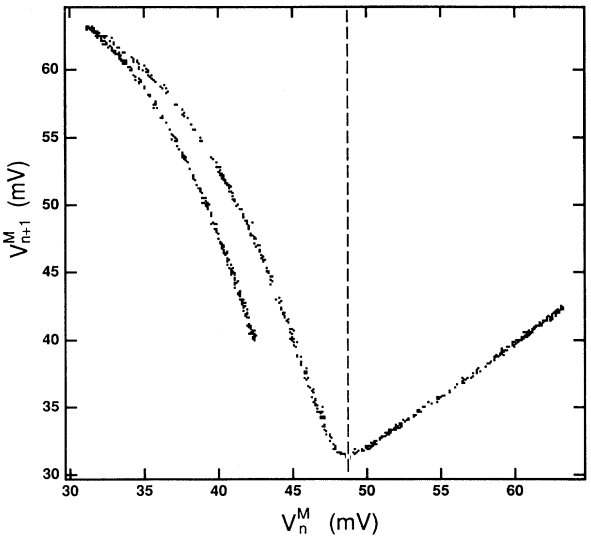

FIG. 4. The first return map of the resonator exhibits a thin structure indicative of one-dimensional mappings. The vertical dotted line divides the map into an unstable region characterized by a slope greater than 1 and a stable one.

IV. CHARACTERIZING SYNCHRONIZATION BY CONDITIONAL LYAPUNOV MULTIPLIERS

In this section, we utilize conditional local and global Lyapunov multipliers in order to characterize the feasibility of control theory synchronization for the diode resonator. Global Lyapunov multipliers quantify the average rate of divergence of neighboring orbits over the entire phase space of the attractor. Local Lyapunov multipliers, on the other hand, characterize the local rate of divergence of neighboring orbits of the attractor along small sections of the orbit. They are dependent on the location of the evaluated point and provide detailed information about the regional stability of the attractor [27,28].

Conditional Lyapunov multipliers have been introduced by Pecora and Carroll [2] and Rul'kov (first reference in [6]). Let us consider the evolution of the difference between two chaotic systems. In a $2k$-dimensional phase space defined by the $\boldsymbol{x}$ and $\boldsymbol{y}$ systems, a synchronization manifold exists for which $\boldsymbol{x}_n = \boldsymbol{y}_n$. The conditional Lyapunov multipliers characterize the evolution of an error signal defined by $\boldsymbol{\epsilon}_n = \boldsymbol{y}_n - \boldsymbol{x}_n$ in a direction perpendicular to this manifold. A linearization of the mapping for this difference yields

$$\boldsymbol{\epsilon}_{n+1} = \boldsymbol{DF}(\boldsymbol{x}_n) \cdot \boldsymbol{\epsilon}_n\ , \tag{4.1}$$

where $\boldsymbol{DF}$ is the Jacobian matrix calculated from the difference between the master and slave mapping functions. The direction of the displacement is given by $\boldsymbol{\epsilon}_n/|\boldsymbol{\epsilon}_n|$ while the magnitude is given by

$$m_n = \frac{|\boldsymbol{\epsilon}_{n+1}|}{|\boldsymbol{\epsilon}_n|}. \tag{4.2}$$

This is referred to as the conditional local Lyapunov

multiplier (CLLM). It expresses the amount of growth ($|m_n| > 1$) or contraction ($|m_n| < 1$) of the error signal perpendicular to the synchronization manifold at a given point $\boldsymbol{x}_n$. Note that in general, the value obtained for m_n is dependent on the direction chosen for the displacement and that for each dimension of the dynamical system there will be a corresponding conditional Lyapunov multiplier. However in the case of the diode resonator, we are interested only in the largest Lyapunov exponent which corresponds to the single unstable direction.

By calculating the evolution of the error signal at each iterate throughout the synchronization manifold, the conditional global Lyapunov multiplier is given by

$$m_g = \lim_{N\to\infty} \left(\prod_{n=0}^{N} \frac{|\epsilon_{n+1}|}{|\epsilon_n|} \right)^{\frac{1}{N+1}} . \tag{4.3}$$

This procedure calculates only the largest multiplier.

Explicitly, the evolution of the error, ϵ_n, is measured by evaluating the propagation of a point along the master trajectory and a nearby point along the slave orbit. The slave orbit is perturbed by the effect of some feedback; otherwise, this calculation would simply be an estimate of the usual Lyapunov multiplier. Synchronization occurs when the corresponding conditional global Lyapunov multipliers are all less than 1.

The significance of the algorithm proposed by Lai and Grebogi for maps is that it provides a technique to calculate and apply perturbations which set the CLLM's along the unstable directions to zero at every iteration. Since the conditional global Lyapunov multiplier will be minimized as well, this technique guarantees synchronization in systems with only one unstable direction. However, the requirement for convergence is only that the conditional global Lyapunov multipliers have a magnitude less than unity. Therefore it is possible to adapt the Lai and Grebogi perturbation formula to obtain a simpler means for determining feedback. In Ref. [9], this meant amplifying $\boldsymbol{y}_n - \boldsymbol{x}_n$ with a constant factor instead of the iterate dependent factors called for in Eq. (2.1).

A numerical calculation of the resonator CLLM's on the Poincaré section is performed by observing the evolution of the error signal between successive piercings. The ratio between the final trajectory difference and the initial one was considered to be the CLLM for the initial piercing. Global Lyapunov multipliers are then obtained by the geometrical averaging method described above. Figure 5 shows the CLLM's versus the peak values of the current. In the event of no applied feedback to the slave orbit, the CLLM's are identical to the local Lyapunov multipliers of the single resonator. This case is shown in Fig. 5(a). The CLLM's are predominantly greater than 1, and as expected synchronization is not achieved. Note that even without applied feedback, CLLM's along the higher peaks are less than 1. Though globally unstable, this shows that the attractor has regions of natural stability.

We next look at amplitude modulating the drive wave of the slave system by the term $\alpha\,[\mathcal{I}^S(t_n) - \mathcal{I}^M(t_n)]$ where α is a *constant* amplification factor and $\mathcal{I}^S$ and $\mathcal{I}^M$ refer to the currents in the slave and free operating master

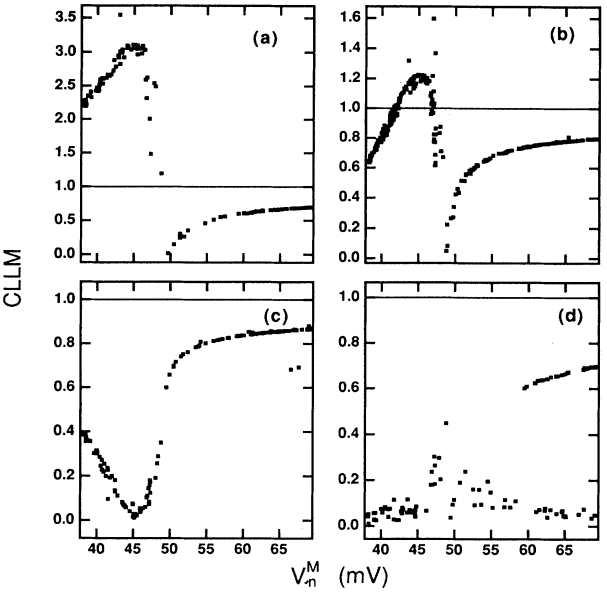

FIG. 5. A numerical calculation of the conditional local Lyapunov multipliers from Eq. (3.1) and Eq. (3.2). (a) The master and slave resonator are operating independently. (b) The feedback amplification factor is taken to be a constant $\alpha = 34$ (α is dimensionless). Though some local multipliers remain greater than unity, the global Lyapunov multiplier is less than unity and synchronization occurs. (c) An optimum constant feedback factor of 57. The perturbation substantially reduces the multipliers in the unstable region of the attractor but does little to influence those in the stable regions. (d) Application of the Lai and Grebogi prescribed feedback factor α_n from Eq. (3.5). This synchronization procedure is the most efficient at minimizing the local Lyapunov multipliers.

resonator at the time of occurrence of the nth peak value, t_n. The first equation of Eq. (3.1) is then modified to

$$\frac{d\mathcal{I}}{d\tau} = \{\mathcal{V}_0 + \alpha\,[\mathcal{I}^S(t_n) - \mathcal{I}^M(t_n)]\}\sin(\tau) + \mathcal{V} - \frac{\mathcal{I}}{\beta} . \tag{4.4}$$

The implementation of Eq. (4.4) was the experiment carried out by the authors and presented in [9]. Figure 5(b) shows the CLLM's when α ($\alpha = 34$) is just sufficient to reduce the multipliers so that synchronization is realized. Even though some of the CLLM's are greater than 1, the global geometric average remains below unity. The CLLM's plotted in Fig. 5(c) are at their least possible values when a constant factor is utilized. In this case $\alpha = 57$.

The iterative dependent term prescribed by the Lai and Grebogi algorithm, Eq. (2.1), presents the optimum choice for the minimization of the conditional multipliers. These are shown in Fig. 5(d). Note that though the CLLM's are largely reduced for the lower values of V^M, they are only slightly affected in the naturally stable regime of the attractor.

Figure 6(a) is a graph of the largest conditional global Lyapunov exponent ($\ln[m_g]$) versus the α. This shows

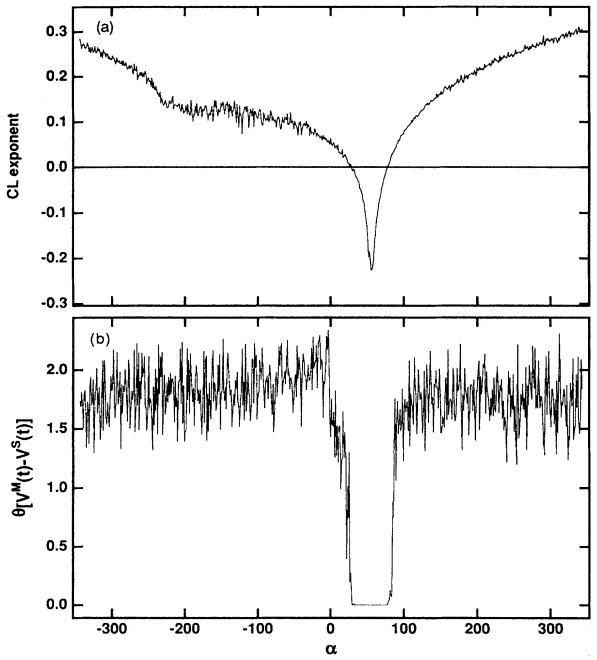

FIG. 6. (a) The largest conditional global Lyapunov exponent versus α shows a band of values for which synchronization can be achieved. (b) The standard deviation, θ, of $\mathcal{I}^{\mathcal{S}} - \mathcal{I}^{\mathcal{M}}$ as the constant feedback synchronizing factor is increased. The plot is in excellent agreement with experimental observations.

the band of constants for which synchronization can be achieved. Figure 6(b) is a plot of the standard deviation of $\mathcal{I}^S - \mathcal{I}^M$. The corresponding synchronization of the master and slave is striking as the standard deviation drops to zero in the band. These plots are a numerical illustration of what the authors observed experimentally and reported in Ref. [9].

V. SYNCHRONIZING THE DIODE RESONATOR

In this section we describe the implementation of the Lai and Grebogi synchronization algorithm to the case of two chaotic diode resonators. From the two chaotic dynamical variables, current ($\mathcal{I}$) and voltage drop across the diode ($\mathcal{V}$), we select the current through the resonator as the observable signal. We evaluate the feedback at the peaks of the current. Therefore we rename the iterative dependent factor as a peak dependent factor so that $\delta p_n = \delta p(t_n)$ where t_n refers to the time of occurrence of the nth current peak. δp_n modulates the amplitude of the drive wave, the chosen control system parameter, for some fraction of the known period so that the drive wave has the form $(\mathcal{V}_0 + \delta p_n)\sin(\tau)$.

The formula for δp_n is given by Eq. (3.5). As discussed in Sec. III, the voltage drop across the diodes in the master and slave circuit are nearly identical for the surface of section defined by the current peaks of the master. Physically, this current is measured as the voltage drop across the resistor element, $V^M(t)$, of the resonator. Using $\mathcal{I}_n^M \to V_n^M$ and $\mathcal{I}_n^S \to V_n^S$ we write Eq. (3.5) as

$$\delta p_n = -\frac{\partial V_{n+1}^M/\partial V_n^M}{\partial V_{n+1}^M/\partial p}\left[V^S(t_n) - V^M(t_n)\right]$$

$$\equiv \alpha_n\left[V_n^S - V_n^M\right], \tag{5.1}$$

where we have defined

$$\alpha_n \equiv -\frac{\partial V_{n+1}^M/\partial V_n^M}{\partial V_{n+1}^M/\partial p} \tag{5.2}$$

evaluated at the $V_n^M \equiv V^M(t_n)$.

Thus we need to calculate and apply in real time the ratio of the slope of the map to the shift. Evaluating these terms experimentally can be accomplished by using the first return maps. Figure 7(a) displays two return maps taken at a drive amplitude of 4.6 and 5.1 V, respectively. Since each return map is composed of approximately 300 points and is contaminated by noise, a curve fit is interpolated to average the fluctuations in nearby points. Both return maps are divided into four sections creating a piecewise continuous curve to which a low order polynomial curve fit is computed for each section.

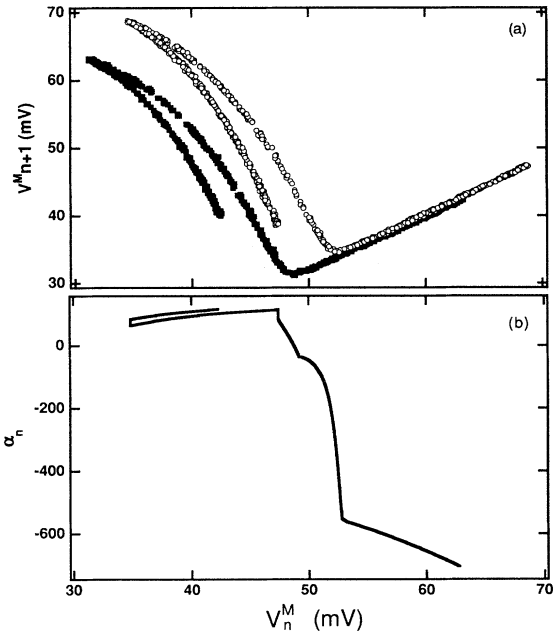

FIG. 7. (a) Two return maps recorded at 4.6 and 5.1 V (upper) superimposed show the effect of a perturbation to the drive wave amplitude. The shift of the map is obtained by measuring the change in peak $\left[V_n^M(5.1\text{ V}) - V_n^M(4.6\text{ V})\right]/0.5$ V. The one-dimensional Jacobian matrix as a function of the peaks is obtained from the slope of the 4.6 V map. (b) The peak dependent feedback amplification factor as a function of the resistor peaks. Below 48 mV the factor is approximately constant regardless of the two lower branches of the return map. Along the upper branch, the factor drops off rapidly due to the shifting of the return maps.

The shift of the map, $\partial V^M_{n+1}/\partial p$, is obtained by considering how the return map reacts to a perturbation applied to the amplitude of the drive voltage. For a driving voltage V_0, we look at how the point $V^S_n(V_0)$, is mapped into V^S_{n+1}. Then at a slightly higher voltage, $V_0 + \Delta V$, we look at how the same point, $V^S_n(V_0)$, is mapped into the new point $V^S_{n+1}(V_0 + \Delta V)$. The shifting is seen in Fig. 7(a). The 5.1 V return map has shifted along the upper branch of the 4.6 V map. The experimental approximation for the shift is then

$$\partial V^M_{n+1}/\partial p \approx \frac{[V^S_{n+1}(V_0 + \Delta V) - V^S_{n+1}(V_0)]}{\Delta V}. \quad (5.3)$$

The iterate dependent amplification factor is the negative of the quotient of the two terms above. Figure 7(b) shows the result of the calculation versus the peaks of $V^M(t)$. While both branches of the lower folded region produce a relatively constant factor, in the upper region the factor drops off rapidly. The return map of the diode resonator shifts along an axis almost parallel to the upper branch and the shift, $\partial V^M_{n+1}/\partial p$, approaches zero. Hence the feedback factor becomes quite large. In this region it is not possible to apply the exact feedback perturbation since the large amplification of the unavoidable noise along with any differences in $V^S(t)$ and $V^M(t)$ would overmodulate the drive wave. A numerical calculation of the feedback factor, shown in Fig. 8, displays a similar shape, but does not drop off as drastically.

The problems caused by an infinitesimal shift of the return map are not particular to this dynamical system. For a generic one dimensional return map it is quite possible that the shifted return map may intersect the unperturbed return map. At the point of intersection, the value of the shift is zero, producing an infinite value for α_n. When such pathologies occur, one either chooses to not apply feedback or approximate the feedback from the nearby regions.

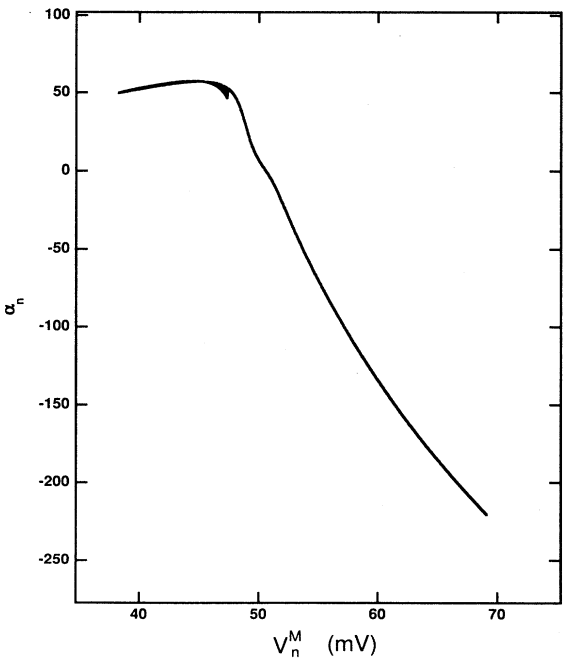

FIG. 8. A numerical calculation of the peak dependent feedback amplification factor is similar to Fig. 7(b). As seen experimentally, the lower section is essentially constant at a value of approximately 57.

By inspecting the first return map (Fig. 4), one notes that the slope of the lower branches is greater than unity while the slope of the upper section is less than 1. Because of the resonator's one-dimensional nature, it follows that the lower section is unstable; nearby orbits in this region diverge. On the other hand, the upper branch is stable and adjacent orbits here should remain temporarily adjacent until the phase space trajectory wanders into the unstable regime. We also point out that the slope, i.e., our approximation for the Jacobian, is equivalent to the CLLM's shown in Fig. 5(a) for the case of no feedback. The salient feature to capitalize upon is that a feedback perturbation need only be applied when the system is in an unstable region of the attractor. In the stable regions feedback perturbations should become unnecessary. For the diode resonator, this means that feedback could be applied only when the resistor voltage peaks are less than 48 mV. In these critical regions, the amplification factor is constant [see Fig. 7(b) and Fig. 8].

VI. SYNCHRONIZATION EXPERIMENTS

A. Setup

In this section, we describe the results of two experiments performed that test control theory synchronization. A block diagram of the experimental arrangement is shown in Fig. 9. The difference in the two voltage signals, $V^S(t_n) - V^M(t_n)$, is multiplied by α_n [Figs. 9(b) or 9(c) described below] and the product is input into a sample and hold amplifier. At $V^M(t_n)$, the feedback is held by the sample and hold device and gated into the amplitude modulation input of the waveform generator which drove the slave resonator. The duration of the feedback can range from 0 μs to within 1 μs of the next cycle — a limitation due to the acquisition time of the sample and hold device. Experimentally adjustable parameters are phase, amplitude, and dc bias differences in the two driving waves, and characteristics of α_n.

B. Synchronization by means of an iterate dependent feedback factor

The goal of this experiment is to synchronize the resonators using the prescribed feedback derived from the control scheme. The calculated feedback curves portrayed in Fig. 7(b) and Fig. 8 are reminiscent of the well known current-voltage curve of rectifier diodes. Hence a rectifier composed of a diode in series with a resistor is used to create the desired factor. Figure 9(b) shows the means of producing this term (solid line). The control of the feedback (dotted line) is unused in this experiment; feedback is always applied at each peak. $V^M(t)$ is ampli-

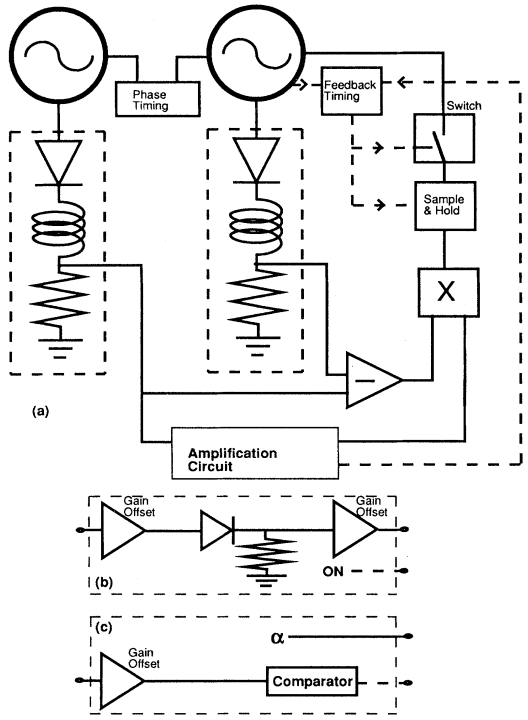

FIG. 9. Schematic diagram of the experiments. (a) $V^S(t) - V^M(t)$ is obtained, muliplied by α_n, then input into the sample and hold amplifier. On the drive wave peaks, the input is frozen and amplitude modulates the slave drive wave generator. (b) By using $V^M(t)$ to drive a diode-resistor rectifier element, the inverted voltage drop across the resistor of the rectifier generates α_n (solid line). The feedback control (dotted line) applies the perturbations for every cycle. (c) If $V^M(t)$ is greater than the threshold voltage of the comparator the feedback procedure is impeded (dotted line). Otherwise α_n is constant and feedback applied.

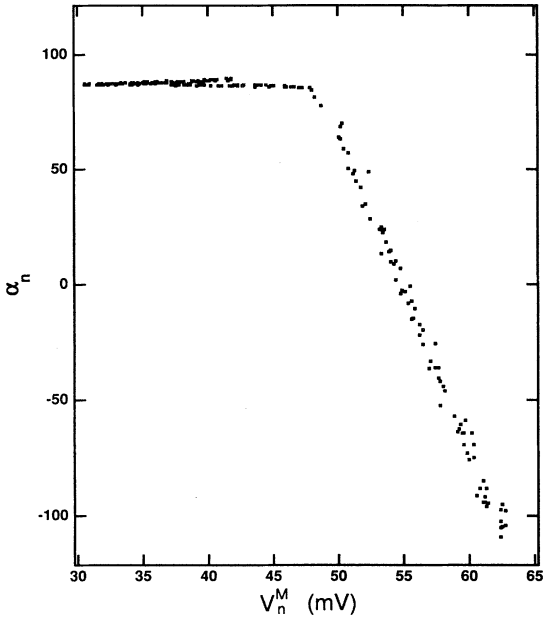

FIG. 10. The experimentally applied α_n is seen by recording the output of the rectifier element on the drive wave peaks. Its form is experimentally adjustable.

fied and dc biased, then used to drive the diode-resistor rectifier. The voltage drop across the rectifier resistor is then inverted, amplified, and dc biased. By adjusting the various gains, the shape of α_n could be varied from a line of slope zero to the desired peak dependent feedback factor. Figure 10 shows the experimentally implemented amplification factor α_n versus $V^M(t_n)$. The composite feedback perturbation is created by multiplying $V^M(t_n) - V^S(t_n)$ by α_n.

In the experiment, feedback amplitude modulates the slave waveform generator for 12 μs of the 14.3 μs period. In contrast to the numerical algorithm of Lai and Grebogi, feedback is applied regardless of the magnitude of δp_n. At time $t = 0$ the feedback is applied. Figure 11(a) shows the time series of $V^M(t)$ and $V^S(t)$. Figure 11(b) plots the difference between the two signals. Even while unsynchronized, perturbations applied to the slave drive wave are relatively small. After 200 μs the two signals are virtually identical. In the optimum case, the ratio of the feedback pulse heights to the amplitude of the drive wave is less than 2%.

When the values of $V^M(t_n)$ are above 48 mV the degree of synchronization is only slightly affected by the magnitude of the feedback factor. The slope of this feedback factor curve (Fig. 10) can be varied from zero to a quite large value, yet synchronization persists. This tolerance is to be expected since, as noted above, the attractor is stable in this regime. A more critical parameter is the overall upwards or downwards shifting of the

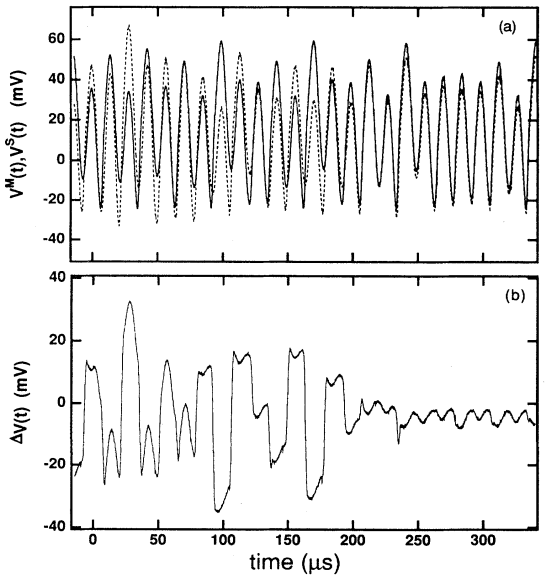

FIG. 11. (a) A time series of $V^M(t)$ (solid line) and $V^S(t)$. Feedback commences at $t = 0$. (b) $\Delta V(t) = V^S(t) - V^M(t)$ plotted in the time domain. Synchronization is achieved in about 175 μs.

feedback curve. Synchronization occurs only for a small range of shifting since it is the constant portion of the factor which critically affects the unstable region of the attractor.

If feedback is applied longer than 12 μs of the 14.285 μs period, synchronization could not be maintained. This observation is in contrast to the hypothesis that feedback should be applied for the entire duration of the period. Since the Lai and Grebogi synchronization scheme was developed for maps, it is natural to assume that in going to a dynamical system, the feedback signal should be applied for the entire period. However, this is not what we observed. As a final note, the minimum amount of time feedback could be applied before synchronization is lost, when initially commencing at the voltage peaks, is 8 μs.

C. Synchronization by applying feedback only when necessary

As a test of the natural stability of the attractor, an experiment was constructed so that feedback is applied only when the diode is operating in unstable regions of the attractor, i.e., when $V^M(t_n) < 48$ mV. This region is seen in Fig. 4. The vertical dotted line delineates the unstable region on the left from the locally stable region to the right. Figure 9(c) is a block diagram of the comparison circuit. The amplification factor (solid line) is constant. The comparator produces a control signal (dotted line) enabling or disabling the feedback timing circuit. Since peaks less than 48 mV occur 64% of the time, feedback is inhibited for more than a third of the sampling periods.

With the threshold set to disable the feedback when $V^M(t_n)$ is above 48 mV, this scheme successfully synchronized the two resonators. The synchronization obtained is equal to that obtained in the first experiment. Figure 12 shows $V^M(t)$, (a), along with the applied feedback, (b), which is scaled as a fraction of the drive wave amplitude. From the graph, one sees that no modulation is applied for the higher peaks. After a period with no applied feedback, the following kick remains relatively small and often smaller than those applied for several periods. This indicates that though the two systems were occasionally drifting apart, they were in a stable region of the attractor. It is possible for synchronization to occur by simply applying the feedback at intervals on the order of the inverse of the Lyapunov exponent since it takes a finite time for the trajectories to diverge. However if this were the case the applied feedback after a nonmodulating period would be large since it is directly proportional to the difference in the two orbits.

By adjusting the threshold level of the comparator, the process could be implemented for any voltage level of $V^M(t)$. Synchronization, as expected, occurs when the cutoff threshold is any value above 48 mV. Synchronization persisted when the cutoff level is reduced to 43 mV. At this level feedback is applied on only 52% of the peaks. Below this level, the feedback is not sufficient to maintain a viable synchronization.

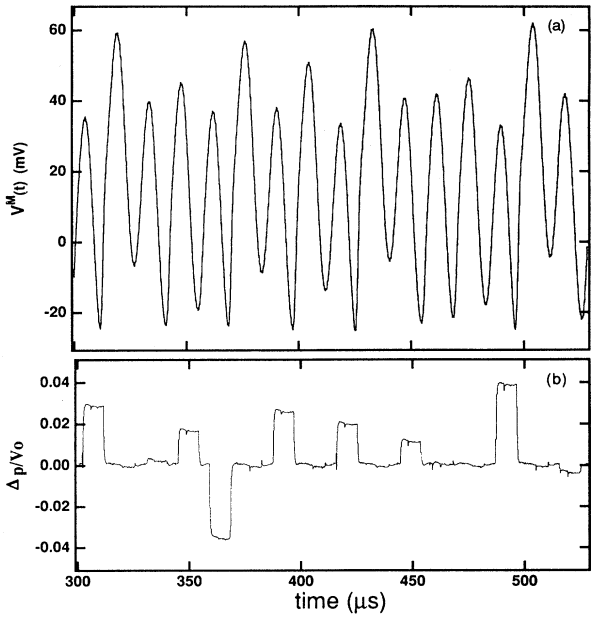

FIG. 12. Synchronization can be obtained when feedback is applied only when necessary. (a) A time series of the chaotic signal $V^M(t)$. (b) The synchronizing feedback, δp. In this case, it is applied only if $V^M(t_n) < 43$ mV.

VII. DISCUSSION AND SUMMARY

In this paper we experimentally implemented the synchronization by control scheme of Lai and Grebogi [8] in a pair of nearly identical chaotic diode resonators. This method locally minimizes the rate of divergence of the two chaotic trajectories upon the crossing of a suitably defined surface of section. As a result, the average global rate of divergence of the chaotic trajectories, as the orbits wander through the attractor, is minimized, and synchronization is ensured. These local and global rates of divergence are, respectively, measured by the conditional local (CLLM) and global Lyapunov multipliers for the Poincaré map defined for the system. From a numerical model and from experimental data we calculated the perturbations necessary to achieve synchronization and explore their effect on the largest conditional Lyapunov multipliers.

In the above method, an iterative dependent proportionality factor α_n multiplied the chaotic signal difference between the master and slave diode resonators at the peaks of the driving voltage in order to form the perturbation necessary to induce synchronization. We were able to calculate α_n from both experimentally and numerically obtained first return maps, which for the case of the diode resonator, are nearly one dimensional. Synchronization was achieved by modulating the drive wave of the slave resonator for a fraction of the period. However, in contrast to our initial expectations, when feedback was applied for more than 85% of the period, the drive wave was overmodulated and synchronization was lost.

A modification of the above method in which the iter-

ative dependent factor α_n is approximated by a constant α across the whole attractor was explored by the authors in [9]. In this paper we demonstrated that for a certain range of values the effect of a constant α is to locally alter the unperturbed local Lyapunov multipliers for the system so that the conditional global Lyapunov multiplier is reduced to a value below unity, thus ensuring global synchronization. For the diode resonator system there are regions of the attractor in which nearby orbits are naturally attracting (magnitude of CLLM < 1) and regions for which the orbits are naturally repelling (magnitude of CLLM > 1). We experimentally demonstrated that synchronization can be achieved by applying perturbations exclusively in the latter region. This represents a very economical approach to synchronization.

The method of synchronization by control discussed in this paper offers an approach to chaotic synchronization that is directly based on concepts successfully employed to control unstable periodic orbits. Its main advantage is that it gives a well defined prescription for obtaining the proportionality factor α_n involved in the perturbation formula. The information required to compute α_n can be derived experimentally from the unperturbed system. The method of synchronization by control is another tool in the workbox of schemes that can be brought to bear on problems involving synchronization.

Since the method of synchronization by control was developed for systems with one positive Lyapunov exponent, a future problem to consider is its extension to more complex dynamical systems. As discussed at the end of Sec. II, the local minimization of the CLLM at each iterate of the Poincaré map is not sufficient to induce synchronization when more than one positive Lyapunov exponent exists. For such systems, synchronization cannot be achieved through a scalar feedback signal. Even for systems with one positive Lyapunov exponent, the method may be difficult to implement if the dynamical system has a phase space of dimension larger than 3 (or 2 for maps). The reasons stem from the method's utilization of the unstable contravariant eigendirection $\boldsymbol{f}_{u(n)}$ at each iterate of the Poincaré map. To compute $\boldsymbol{f}_{u(n)}$ one needs a representation of all the stable and unstable eigendirections at each iterate. This, in general, can be difficult to find if the Poincaré map has dimension greater than 2 [29]. Nonetheless, if some method can be employed to estimate $\boldsymbol{f}_{u(n)}$ by other means, the synchronization by control scheme will yield an explicit perturbation formula capable of inducing synchronization between chaotic trajectories.

ACKNOWLEDGMENTS

The authors would like to thank Jose Perez for valuable discussions concerning the diode resonator. T.C.N. and V.K. would like to thank G.P. Tsironis for making his collaboration possible. T.C.N. wishes to thank the Air Force Office of Scientific Research for support. P.M.A. wishes to thank the National Research Council for supporting this work.

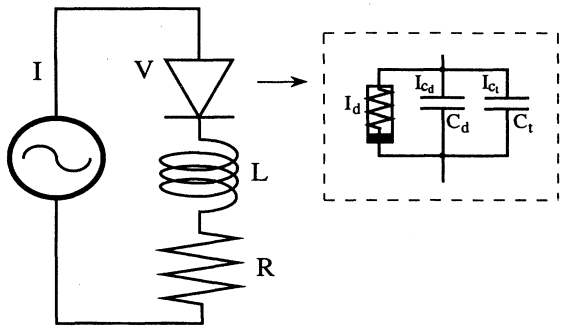

FIG. 13. The diode resonator and a model of the diode. The diode is represented by a nonlinear resistance in parallel with nonlinear space-charge and diffusion capacitances.

APPENDIX

The diode can be modeled as a nonlinear resistor in parallel with nonlinear capacitors (see Fig. 13). The nonlinear resistance of the diode describes the well known current-voltage characteristics given by the Shockley equation, $I_d = I_s[\exp(eV/nkT) - 1]$, where I_s is the reverse bias saturation current, e/kT is the thermal voltage, and n is an emission coefficient implemented to take into account carrier recombination in the depletion zone.

The capacitance terms are modeled from a consideration of the applied ac signal. Charge carrier recombination near the p-n junction creates a depletion region populated primarily by immobile charges. On application of a bias voltage injected charge moves into or out of the depletion region altering its width. This variance induces a nonlinear depletion (or space-charge) capacitance which can be thought of as a parallel plate capacitance with a voltage dependent width. While the diode is reversed biased, this term is given by $C_t = C_b/(1-V/V_J)^m$, where V_J is the junction potential, C_b is the zero voltage bias capacitance, and m, the grading coefficient, refers to the variation of the doping concentration across the p-n junction. Since this term would become infinite when $V = V_J$, it is used whenever $V < V_J/2$. A forward bias modification of the capacitance applied whenever $V \geq V_J/2$ is $C_t = C_b\,(b_1 + mV/V_J)/b_2$ where b_1 and b_2 are parameters to ensure continuity of the capacitance, $b_1 = (1-m)/2$ and $b_2 = (1/2)^{(1+m)}$. The latter formula is derived from a curve fit to experimental data and is valid as long as the forward applied voltage is not excessively high [23].

In addition to the space-charge capacitance, a second capacitive effect arises when the finite response time of the mobile charges to the changing field is considered. The variance of this charge with respect to the voltage defines this capacitance: $C_d = C_0 \exp(eV/nkT)$.

With the transformations $\mathcal{I} = I\omega L/V_J$, $\mathcal{V} = V/V_J$, $\mathcal{V}_0 = V_0/V_J$, $\beta = \omega L/R$, $\alpha = eV_J/(nkT)$, $\gamma = \beta I_s R/V_J$, $c_1 = R\beta\omega C_0$, $c_2 = C_b/C_0$, and $\tau = \omega t$, the governing differential equations are transformed into the dynamical equations given in Eq. (3.1). The parameters for the 1N4004 diode are $V_J = 0.34$ V, $I_s = 5.86 \times 10^{-6}$ A, $n = 1.7$, $C_b = 52.1$ pF, $m = 0.38$, and $C_0 = 668$ pF.

[1] E. Ott, C. Grebogi, and J. A. Yorke, Phys. Rev. Lett. **64**, 1196 (1990).
[2] L.M. Pecora and T.L. Carroll, Phys. Rev. Lett. **64**, 821 (1990); Phys. Rev. A **44**, 2374 (1991).
[3] S. Hayes, C. Grebogi, and E. Ott, Phys. Rev. Lett. **70**, 3031 (1993); K.M. Cuomo and A.V. Oppenheim, *ibid.* **71**, 65 (1993); H.D.I. Abarbanel and P.S. Linsay, IEEE Trans. Circ. Sys. II **40**, 643 (1993); S. Hayes, C. Grebogi, E. Ott, and A. Mark, Phys. Rev. Lett. **73**, 1781 (1994).
[4] H.G. Winful and L. Rahman, Phys. Rev. Lett. **65**, 1575 (1990).
[5] A. Garfinkel, M.L. Spano, W.L. Ditto, and J. Weiss, Science **257**, 1230 (1992); S.J. Schiff, K.J. Jerger, D.H. Duong, T. Chang, M.L. Spano, and W.L. Ditto, Nature **370**, 615 (1994).
[6] N.F. Rul'kov, A.R. Volkovski, A. Rodriguez-Lozano, E. Del Rio, and M.G. Velarde, Int. J. Bifurc. Chaos **2**, 669 (1992); K. Pyragas, Phys. Lett. A **181**, 203 (1993); **170**, 421 (1992); T.C. Newell, P.M. Alsing, A. Gavrielides, and V. Kovanis, Phys. Rev. E **49**, 313 (1994); R. Roy and K.S. Thornburg, Jr., Phys. Rev. Lett. **72**, 2009 (1994); D.J. Gauthier, D.W. Sukow, H.M. Concannon, and J.E.S. Socolar, Phys. Rev. E **50**, 2343 (1994); J.E.S. Socolar, D. W. Sukow, and D.J. Gauthier, *ibid.* **50**, 3245 (1994).
[7] T. Shinbrot, C. Grebogi, E. Ott, and J.A. Yorke, Nature **363**, 411 (1993); P.M. Alsing, A. Gavrielides, and V. Kovanis, Phys. Rev. E **50**, 1968 (1994); R. Roy, Z. Gills, and K.S. Thornburg, Opt. Photon. News **5**, 8 (1994).
[8] Y.C. Lai and C. Grebogi, Phys. Rev. E **47**, 2357 (1993).
[9] T.C. Newell, P.M. Alsing, A. Gavrielides, and V. Kovanis, Phys. Rev. Lett. **72**, 1647 (1994).
[10] Y.C. Lai, M. Ding, and C. Grebogi, Phys. Rev. E **47**, 86 (1993).
[11] P. So, E. Ott, and W.P.Dayawansa, Phys. Lett. A **176** 421 (1993); P. So, E. Ott, and W.P. Dayawansa, Phys. Rev. E **49**, 2650 (1994).
[12] E. R. Hunt, Phys. Rev. Lett. **67**, 1953 (1991).
[13] P.S. Linsay, Phys. Rev. Lett. **47**, 1349 (1981).
[14] J. Perez and C. Jeffries, Phys. Lett. **92A**, 82 (1982).
[15] C. Jeffries and J. Perez, Phys. Rev. A **26**, 2117 (1982).
[16] R.W. Rollins and E.R. Hunt, Phys. Rev. A **29**, 3327 (1984).
[17] R. Hilborn, Phys. Rev. A **31**, 378 (1985).
[18] J. Testa, J. Perez, and C. Jefferies, Phys. Rev. Lett. **48**, 714 (1982).
[19] S.D. Brorson, D. Dewey, and P.S. Linsay, Phys. Rev. A **28**, 1201 (1983).
[20] R.V. Buskirk and C. Jeffries, Phys. Rev. A **31**, 3332 (1985).
[21] J. Cascais, R. Dilao, and A. Noronha Da Costa, Phys. Lett. **93A**, 213 (1983).
[22] I. Balberg and H. Arbell, Phys. Rev. E **49**, 110 (1994).
[23] See, e.g., *Semiconductor Device Modelling with SPICE*, edited by P. Antognetti and G. Massobrio (McGraw-Hill, New York, 1988).
[24] Z. Yu, J. Steinshnider, C.L. Littler, J.M. Perez, and J.M. Kowalski, Phys. Rev. E **49** 220 (1994).
[25] The conduction of the diode is quite dependent on the doping concentrations and the ambient temperature. For this reason, quantitative agreement between the model and experiment is not likely unless one measures the pertinent parameters directly from each diode used.
[26] J.L. Kaplan and J.A. Yorke, in *Functional Differential Equations and Approximations of Fixed Points*, Vol. 730 of *Lecture Notes in Math*, edited by Heinz-Otto Peitten and Heinz-Otto Walter (Springer, New York, 1979), p. 228.
[27] H.D.I. Abarbanel, R. Brown, and M.B. Kennel, Int. J. Nonlinear Sci. **2**, 343 (1992).
[28] H.D.I. Abarbanel, R. Brown, J.J. Sidorowich, and L.S. Tsimring, Rev. Mod. Phys. **65**, 1331 (1993).
[29] Y.C. Lai and C. Grebogi, Phys. Rev. E **50**, 1894 (1994).